

# PyAtoms: An interactive tool for rapidly simulating atomic scanning tunneling microscopy images of 2D materials, moiré systems and superlattices

C. Gutiérrez and A. G. Prado

Department of Physics and Astronomy, University of California, Los Angeles,  
Los Angeles, California, 90095 USA

E-mail: [gutierrez@physics.ucla.edu](mailto:gutierrez@physics.ucla.edu)

## Abstract.

We present PyAtoms, an interactive open-source software that quickly and easily simulates atomic-scale scanning tunneling microscopy (STM) images of two-dimensional (2D) layered materials, moiré systems, and superlattices. Rooted in a Fourier-space description of ideal atomic lattice images, PyAtoms is a Python-based graphical user interface (GUI) with robust capabilities for tuning lattice parameters (lattice constants, strain, number of layers, twist angles) and STM imaging parameters (pixels, scan size, scan angle) and provides time estimates for spectroscopic measurements. These capabilities allow users to efficiently plan time-consuming STM experiments. We provide an overview of PyAtoms' current features, describe its underlying mathematical principles, and then demonstrate simulations of several 2D materials including graphene with variable sub-lattice asymmetry, twisted tri-layer graphene moiré systems, and charge- and bond-density wave systems (*2H*-NbSe<sub>2</sub>, *1T*-TaS<sub>2</sub>, Kekulé-distorted graphene, K<sub>0.3</sub>MoO<sub>3</sub>). Finally, we show that PyAtoms can be used as a useful educational tool in entry- and senior-level physics courses.

## 1. Introduction

Scanning tunneling microscopy (STM) [1] is a powerful technique for investigating the atomic-scale electronic and structural properties of materials [2]. In STM, an atomically sharp tip is rastered across a conductive sample surface while recording the current of electrons tunneling from the tip to the sample, or vice versa. The tunneling current is proportional to the energy-integrated local density of states (LDOS), and can thus provide valuable insights into the spatially-dependent electronic properties of novel quantum materials such as high-temperature superconductors [3, 4], charge- or bond-density wave systems [5, 6, 7], and two-dimensional (2D) van der Waals structures and moiré superlattices [8, 9, 10, 11, 12, 13, 14, 15, 16, 17, 18].

A drawback of STM measurements is that they are notoriously time-consuming: Depending on the particular imaging mode (topography or spectroscopy), the time to complete a measurement can take minutes to several *days*. In a STM topography measurement, the STM tip rapidly scans the surface (typical scan rate of  $\sim 1$  Hz) at a single tunneling energy while recording the tunnel current line-by-line; in a STM spectroscopy measurement, the tunnel current and/or the differential conductance,  $dI/dV_b \propto \text{LDOS}(eV_b)$ , (where  $I$  is the tunnel current,  $V_b$  is the voltage bias, and  $e$  is the elementary charge), is *slowly* measured pixel-by-pixel at one or several tunneling energies. The choice of spatial resolution is especially important for spectroscopic measurements, where the Fourier-transformed STM (FT-STM) image can display intricate electronic scattering patterns – called quasi-particle interference (QPI) patterns – that are directly related to constant energy cuts of the momentum-resolved electronic band structure [4, 19]. The significant time commitment of STM imaging in real- or reciprocal-space thus makes it absolutely crucial for researchers to somehow determine the suitable imaging parameters *prior* to engaging a long-term measurement. This would require a tool that could easily simulate STM data in real- and Fourier-space for a variety of quantum material families while also providing real-time estimation of the measurement time.

To address this need, we created PyAtoms: an open-source, Python-based graphical user interface (GUI) equipped with robust capabilities for quickly and easily simulating STM images of several types of 2D van der Waals quantum materials, including graphene, transition metal dichalcogenides, and systems with superlattices such as charge density waves and multi-layered moiré lattices. PyAtoms relies on a simplified model of an ideal atomic lattice, enabling the simulation of STM images for several families of quantum materials and allowing users to tune lattice

strain and sublattice asymmetries. A notable strength of PyAtoms is its unique ability to rapidly simulate even complex STM and FT-STM moiré patterns in real-time. Users can use PyAtoms to quickly determine the local twist and/or lattice mismatch in their experimental data. Moreover, owing to its user-friendly GUI, we have found that PyAtoms is a valuable educational tool for teaching concepts related to periodic structures in real and reciprocal space. PyAtoms is thus a versatile and accessible software tool that can be utilized for novice and advanced 2D material researchers and educators.

To our knowledge, no other software exists that combines PyAtoms’ level of 2D quantum material STM image simulation with a real-time GUI. Gwyddion [20], a versatile scanning probe microscopy (SPM) data analysis software, contains a module for simulating well-known surfaces (square, triangular, silicon  $7 \times 7$ ), but it lacks real-time simulation of multi-layer systems or for tuning strain or sublattice strength. Stephens and Hollen have shared a Matlab GUI for simulating moiré patterns using dot lattices that simultaneously display the Fourier transform [21]. de Jong has shared a very impressive lattice and moiré atomic simulator that allows for tuning the symmetry, strain, and sublattice, but it lacks a real-time GUI [22]. Finally, we note that, while PyAtoms is based on idealized atomic lattices, the National Institute of Standards and Technology (NIST) Joint Automated Repository for Various Integrated Simulations (JARVIS) database hosts a robust library of STM images calculated from density functional theory (<https://jarvis.nist.gov/jarvisstm>) [23].

PyAtoms is built on Python 3 and utilizes widely used libraries such as NumPy [24], SciPy [25], Matplotlib [26] and PyQt5 (<https://www.riverbankcomputing.com/software/pyqt>). These libraries are readily available through common platforms such as Anaconda (<https://www.anaconda.com>). PyAtoms is hosted on Github (<https://github.com/asariprado/PyAtoms>) and is regularly updated. PyAtoms runs on both Windows and MacOS systems, however its compatibility with Linux systems has not been tested.

The article is organized as follows: We first describe the theoretical underpinnings of PyAtoms. We describe how it generates single lattices of various geometries (square, triangular); how we approximate images of moiré and superlattice systems; and how strain and low-pass filtering affect the generated lattice images. We then describe the PyAtoms graphical interface before concluding with its applications in research and education.

## 2. Methods

### 2.1. The ideal atomic lattice

The topographic intensity,  $T$ , of an ideal crystal at position  $\mathbf{r} = (x, y)$  can be expressed as a Fourier sum [27, 28],

$$T(\mathbf{r}) = \sum_k A_k e^{i\mathbf{g}_k \cdot (\mathbf{r} - \mathbf{r}_0)}, \quad (1)$$

where  $\mathbf{g}_k$  corresponds to the  $k^{\text{th}}$  reciprocal lattice vector corresponding to a Bragg reflection, and  $A_k$  are the corresponding Fourier amplitudes for the  $k^{\text{th}}$  mode which, in general, may be complex [27], and  $\mathbf{r}_0$  is the location of the maxima of a reference atom in the image. For the sake of brevity in the following, we assume this reference atom is located at the origin  $\mathbf{r}_0 = (0, 0)$ . For a real image ( $A_k = A_{-k}$ ), the image intensity is thus given by:

$$T(\mathbf{r}) = \sum_k 2A_k \cos(\mathbf{g}_k \cdot \mathbf{r}). \quad (2)$$

For a square lattice with lattice constant  $a$ , there are two reciprocal lattice vectors:

$$\mathbf{g}_1^{sq} = \frac{2\pi}{a} \hat{x}, \quad \mathbf{g}_2^{sq} = \frac{2\pi}{a} \hat{y} \quad (3)$$

For a triangular lattice, the reciprocal lattice vectors are:

$$\begin{aligned} \mathbf{g}_1^{tri} &= \frac{2\pi}{a} \left[ \hat{x} + \frac{1}{\sqrt{3}} \hat{y} \right], & \mathbf{g}_2^{tri} &= \frac{2\pi}{a} \left[ -\hat{x} + \frac{1}{\sqrt{3}} \hat{y} \right], \\ \mathbf{g}_3^{tri} &= -(\mathbf{g}_1^{tri} + \mathbf{g}_2^{tri}). \end{aligned} \quad (4)$$

The ideal square lattice is thus given by

$$T_{\square}(\mathbf{r}) = N_1 + N_2 [\cos(\mathbf{g}_1^{sq} \cdot \mathbf{r}) + \cos(\mathbf{g}_2^{sq} \cdot \mathbf{r})], \quad (5)$$

and the ideal triangular lattice can then similarly be given by

$$T_{\triangle}(\mathbf{r}) = N_1 + N_2 \sum_{k=1}^3 \cos(\mathbf{g}_k^{tri} \cdot \mathbf{r}), \quad (6)$$

Here,  $N_i$  are constants ensuring the normalization of the images, such that  $0 \leq T(\mathbf{r}) \leq 1$ . Including higher harmonics of  $\mathbf{g}_k$  (i.e. more Bragg peaks) in the sum in Eqs. 5, 6 will produce atoms that are more localized in space, approaching Dirac delta functions as the number of harmonics increases [21, 22].

To simulate an arbitrary rotation,  $\theta$ , of the scan axis or a twist angle between two layers, we use the standard 2D rotation matrix:

$$\mathbf{R}_{\theta} = \begin{pmatrix} \cos \theta & -\sin \theta \\ \sin \theta & \cos \theta \end{pmatrix} \quad (7)$$

To apply a uniform rotation by  $\theta$  to the lattice, each of the reciprocal lattice vectors,  $\mathbf{g}_k$ , is rotated to new positions,  $\mathbf{g}'_k$ , individually:

$$\mathbf{g}'_k = \mathbf{R}_{\theta} \mathbf{g}_k \quad (8)$$

### 2.2. Honeycomb crystal structures

The honeycomb crystal, such as that in graphene, consists of a triangular Bravais lattice with a two-atom basis. It can be easily pictured as two interpenetrating triangular Bravais lattices, labeled  $A$  and  $B$  (Fig. 1(a)). Ignoring normalization for the moment, the  $A$  sublattice centered at the origin,  $\mathbf{r}_0 = (0, 0)$ , and with amplitude  $\alpha$  is given by

$$T_A = \alpha \sum_k \exp(i\mathbf{g}_k^{tri} \cdot \mathbf{r}). \quad (9)$$

The  $B$  sublattice centered at the nearest-neighbor distance  $\mathbf{s} = (a/\sqrt{3})\hat{y}$  with respect to the  $A$  sublattice, and with amplitude  $\beta$ , is given by

$$T_B = \beta \sum_k \exp[i\mathbf{g}_k^{tri} \cdot (\mathbf{r} + \mathbf{s})] = \beta e^{2\pi i/3} \sum_k \exp(i\mathbf{g}_k^{tri} \cdot \mathbf{r}), \quad (10)$$

Here, we use the fact that  $\mathbf{g}_k^{tri} \cdot \mathbf{s} = 2\pi/3 \pmod{2\pi}$  for each  $k$ . The most general honeycomb crystal (centered at an  $A$  sublattice site) is thus given by the sum,

$$T_{AB} = T_A + T_B = (\alpha + \beta e^{-2\pi i/3}) \sum_k \exp(i\mathbf{g}_k^{tri} \cdot \mathbf{r}). \quad (11)$$

The properly normalized atomic honeycomb image is then expressed as:

$$T_{\circlearrowleft} = N_1 + N_2 \Re\{T_{AB}\}, \quad (12)$$

where  $\Re\{T_{AB}\}$  denotes the real part of  $T_{AB}$ , and  $N_i$  are constants such that  $0 \leq T_{\circlearrowleft} \leq 1$ . Shifting the origin to a  $B$ -site atom or honeycomb hollow site amounts to multiplying  $T_{AB}$  in Eq. 6 by a phase shift of  $e^{-2\pi i/3}$  or  $e^{-4\pi i/3}$ , respectively. A triangular lattice is recovered when  $\alpha$  or  $\beta$  is set to zero.

Figure 1 displays several simulated STM images of a honeycomb crystal centered at a hollow (H) site. Ideal graphene (lattice constant  $a = 0.246$  nm) is simulated when the amplitudes of the  $A$  and  $B$  sublattices are equal (Fig. 1(a)). A vertical line cut of the simulated image (Fig. 1(b)) shows that the honeycomb crystal (solid black line) is composed of two triangular lattices, with atoms from each lattice centered at  $A$  (solid red line) and  $B$  (solid blue line). Modifying the relative amplitudes of the two sublattices ( $\alpha, \beta$ ) can create simulated STM images of more general honeycomb structures (Fig. 1(c)). This can be used to model STM images of transition metal dichalcogenides, graphene with broken sublattice

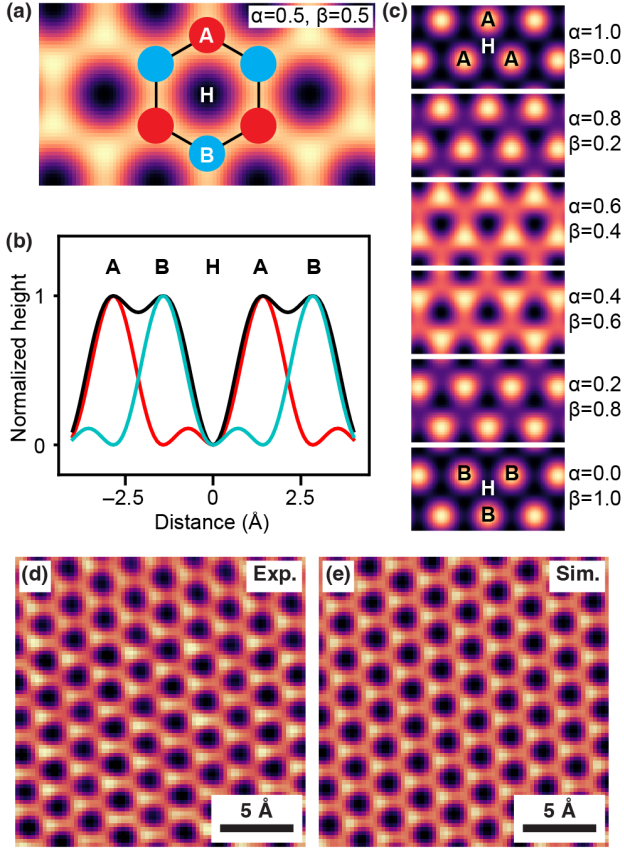


**Figure 1. Generalized triangular lattices.** (a) PyAtoms simulated image of graphene ( $a = 2.46 \text{ \AA}$ ) created with equal amplitude sublattices ( $\alpha = \beta = 0.5$ ). (b) Vertical line scan of the image in (a) connecting consecutive hollow sites. (c) Series of simulated generalized honeycomb crystals with variable amplitudes on each sublattice. (d) Experimental STM image ( $V_b = -400 \text{ mV}$ ,  $I_t = 250 \text{ pA}$ ,  $T = 4.7 \text{ K}$ ) of graphite displaying sublattice asymmetry. (e) PyAtoms simulation of (d) ( $\alpha = 0.45, \beta = 0.55$ ) that faithfully reproduces the sublattice asymmetry.

symmetry, or experimental STM images recorded with an asymmetric tip. The relative sublattice strength ( $\alpha, \beta$ ) and the image origin (A, B, or hollow site) is easily implemented using PyAtoms’s GUI (Fig. 3(a)).

As an example of PyAtoms’ robust capabilities, consider Fig. 1(d), which displays an experimental STM image of the surface of graphite. Typically, the surface of graphite appears in STM as a triangular lattice [1, 29]. The presence of the other sublattice is thus an artifact, most likely due to an asymmetric or doubled STM tip. This is easily simulated with PyAtoms in Fig. 1(e) by choosing sublattice parameters ( $\alpha = 0.45, \beta = 0.55$ ).

### 2.3. Superlattices and multi-layered systems

A superlattice is a larger periodic structure that is superimposed over an existing lattice. Superlattices

can emerge from surface reconstructions [1], alloys and interfaces of materials [30], the presence of periodic lattice distortions and/or charge- or bond-density waves [5, 6, 31, 32], or, in moiré systems, from the combination of two or more crystal lattices [8, 9, 10, 11, 12, 13, 14, 15, 16, 17]. The moiré superlattice (wavevectors  $\mathbf{g}_{M,i}$ ) can be understood as the real-space periodic analog of the beat-frequency in sound: Interference between two periodic lattices (labeled A and B with wavevectors  $\mathbf{g}_{A,i}$  and  $\mathbf{g}_{B,i}$ ) will create a moiré superlattice with a wavevector given by the difference,  $\mathbf{g}_{M,i} = \mathbf{g}_{A,i} - \mathbf{g}_{B,i}$ . The smaller the difference between the two lattices – either in magnitude or direction, i.e. twist – the smaller the moiré wavevector, and thus the longer the real-space wavelength,  $\lambda_M \propto |\mathbf{g}_M|^{-1}$ . The presence of this long-wavelength moiré periodic potential can have a dramatic effect on the electronic properties of 2D material stacks, from inducing superconductivity to correlated insulating behavior and magnetism [33, 34, 35, 36, 37].

In PyAtoms, we currently employ two models that simulate the vast majority of scanning probe images of atomic superlattices in both real- and reciprocal-space. **Toy or “Simple” model:** This is a minimal toy model that yields a superlattice that is given by,

$$T_M^S \propto (1 - \eta) \sum_{l=1} T_l + \eta \prod_{l=1} T_l. \quad (13)$$

Here,  $T_M^S$  represents the moiré or other superlattice image,  $T_l$  represents the individual constituent lattices, and  $\eta$  is a parameter ( $0 \leq \eta \leq 1$ ) that weighs the relative strength of the sum of the lattices,  $\sum_l T_l$ , to their product,  $\prod_l T_l$ . Our toy model has notable strengths: (i) a single toy parameter,  $\eta$ , that is GUI-friendly; (ii) it creates real-space simulations with a wide tuneability in the image contrast to best compare with experimental data; and (iii) low-pass filtering of the resultant image agrees with experimental data (described below and Fig. 2f). We note that, with this model, the FT-STM image — by design — contains only first-order Bragg and superlattice peaks, which is typical of most experimental STM data [7, 9, 10, 38].

**Tunneling or “Log” model:** An alternative model proposed by Joucken *et al* [38] for simulating multi-layer moiré superlattices is rooted in the STM constant-current tunneling process and additionally takes into account the inter-atomic layer spacing,  $d$ , and the out-of-plane exponential decay length,  $\lambda$ . Here, the STM tunnel current is given by,

$$I(x, y, z) \propto e^{-z(x,y)/\lambda} \sum_{l=1} T_l e^{-(l-1)d/\lambda}, \quad (14)$$

where  $z(x, y)$  is the STM tip height at lateral position  $(x, y)$  and  $T_l$  ( $l = 1, 2, \dots$ ) describes the LDOS



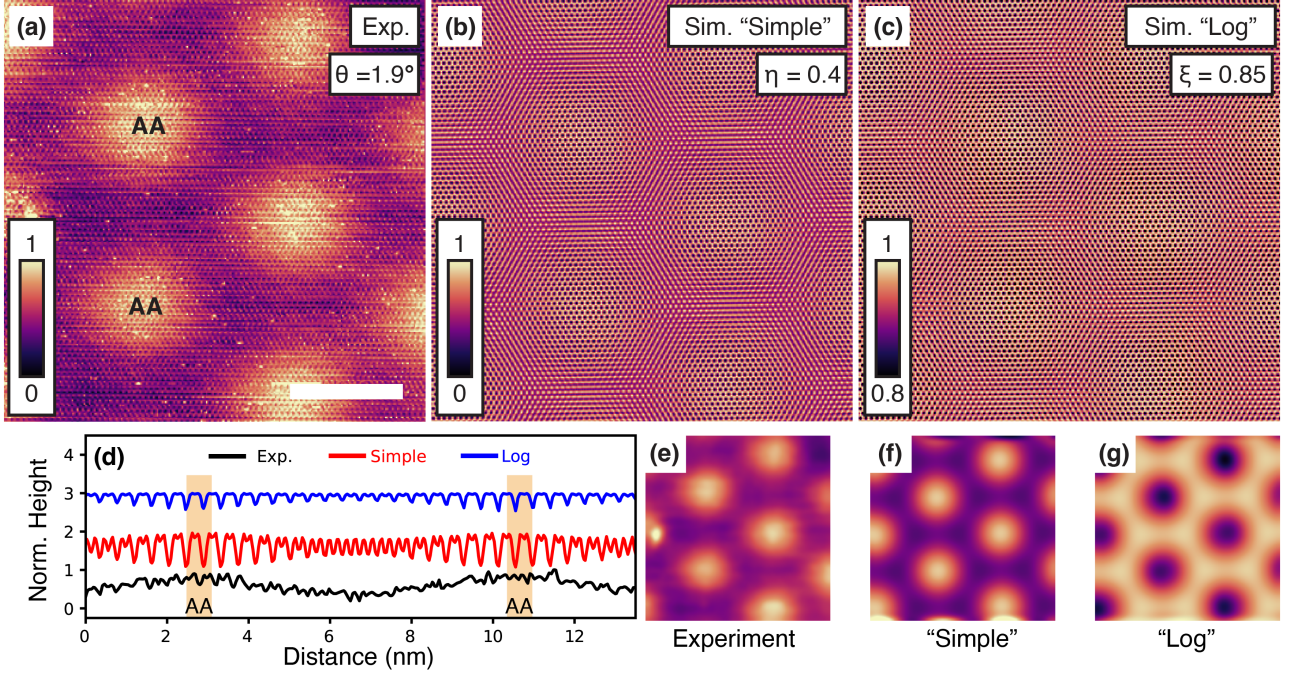


**Figure 2. Moiré simulations of experimental data.** (a) Experimental STM image of twisted graphene-graphite with a moiré twist of  $\theta = 1.9^\circ$ . ( $V_b = -400$  mV,  $I_t = 250$  pA,  $T = 4.7$  K). The height has been normalized to  $[0, 1]$ . (b) Simulation using the “simple” moiré model with  $\theta_{12} = 1.9^\circ, \eta = 0.4$ . (c) Same as (b) using the “log” moiré model with  $\xi = 0.85$ . Note the compressed color scale. (d) Linecuts between the two AA moiré sites in (a)-(c). (e-f) Same as (a-c) after low-pass filtering ( $\sigma = 6$  pixels) which highlights the differences between the simulated moiré models. All images have a lateral size of  $18.7 \text{ nm} \times 18.7 \text{ nm}$ .

in the  $l$ th atomic layer from the surface. In an STM constant-current measurement, the tip height,  $z(x, y)$ , changes dynamically to maintain a constant tunnel current,  $I(x, y, z)$ , through a feedback-loop. Setting the left-hand side of Eq. 14 constant and solving for the tip height,  $z(x, y)$ , yields the resultant superlattice STM topographic height image,  $T_M^L = z(x, y)$ , given by

$$T_M^L \propto \ln \left| \sum_l T_l e^{-(l-1)d/\lambda} \right| \propto \ln \left| \sum_l T_l e^{-(l-1)\xi} \right|, \quad (15)$$

where, in the last line, we have combined the ratio of the inter-layer distance ( $d$ ) to the decay length ( $\lambda$ ) into a single, GUI-friendly parameter,  $\xi = d/\lambda$ :  $\xi$  small corresponds to a short interlayer distance (or long atomic decay length);  $\xi$  large corresponds to a large interlayer distance (or short atomic decay length). This model has its own notable strengths: (i) a single parameter,  $\xi$ , that is GUI-friendly; (ii) the relative intensity of constituent lattices can be tuned by adjusting  $\xi$ , and (iii) the Fourier-transformed image contains all orders of the superlattice peaks. However, the logarithm in Eq. 15, strongly affects the simulated image’s dynamic range which makes adjusting the contrast to match experimental data much more difficult. By allowing the user to toggle between the two models (“Simple” or “Log”), the user

can determine the model and parameters to best match their experiment. Future versions of PyAtoms can easily allow even more models. However, we must stress that PyAtoms provides simulations of the ideal moiré lattices and cannot account for lattice relaxation [39].

Figure 2 contrasts the two models. Shown in Fig. 2(a) is an experimental STM image recorded on graphite at  $T = 4.7$  K. The presence of a moiré pattern indicates the delamination and twisting of the top-most graphene layer [40, 41]. The twist angle can be determined from the moiré wavelength using well-known geometric relations which yields  $\theta_{12} \approx 1.9^\circ$ . Alternatively, the parameter can be determined using PyAtoms, which can rapidly simulate the data as shown in Fig. 2(b,c) using either the “Simple” or “Log” model. The key differences between the two models can be seen by taking a linecut connecting the moiré AA sites (Fig. 2(d)). The “Simple” model (red line) has an amplitude similar to that in experiment (black line). The “Log” model (blue line), however, has a much narrower height range and, owing to Eq. 15, additionally features deep minima at the AA sites. Low-pass filtering the experimental and simulated images (Fig. 2(e)-(g)) shows that the “Simple” model more closely follows the experimental moiré image while the “Log” model yields an inverted

filtered image owing to the deep minima at the AA sites.

#### 2.4. Homogeneous strain

Strain is a powerful experimental method to tune electronic and optical properties of materials. When a crystal lattice is strained, the atomic bonds in real-space become distorted, consequently shifting the reciprocal lattice vectors. This can drastically alter a material's electronic properties by distorting the shape of the Fermi surface and the Brillouin zone boundaries, affecting the vibrational properties, and even opening of band gaps in the band structure [42].

To leading order in the strain tensor,  $\epsilon$ , the presence of strain affects the direct lattice vectors via

$$\mathbf{v} = (\mathbb{I} + \epsilon)\mathbf{v}_0, \quad (16)$$

where  $\mathbf{v}_0$  is the un-strained direct lattice vector,  $\mathbf{v}$  is the strained direct lattice vector,  $\mathbb{I}$  is the  $2 \times 2$  identity matrix, and  $\epsilon$  is the two-dimensional strain tensor given by

$$\epsilon = \begin{pmatrix} \epsilon_{xx} & \epsilon_{xy} \\ \epsilon_{yx} & \epsilon_{yy} \end{pmatrix}. \quad (17)$$

In PyAtoms, the strain  $\hat{x}$ -axis is directed along the first direct lattice vector  $\mathbf{a}_1 = a\hat{x}$ . The resulting strain-distorted reciprocal lattice vectors are given by (to leading order in  $\epsilon$ ),

$$\mathbf{g}_1^{sq} \approx \frac{2\pi}{a} [(1 - \epsilon_{xx})\hat{x} - \epsilon_{xy}\hat{y}] \quad (18)$$

$$\mathbf{g}_2^{sq} \approx \frac{2\pi}{a} [-\epsilon_{xy}\hat{x} + (1 - \epsilon_{yy})\hat{y}] \quad (19)$$

for the square lattice and

$$\mathbf{g}_1^{tri} \approx \frac{2\pi}{a} \left[ \left(1 - \epsilon_{xx} - \frac{\epsilon_{xy}}{\sqrt{3}}\right)\hat{x} + \left(\frac{1}{\sqrt{3}} - \epsilon_{xy} - \frac{\epsilon_{yy}}{\sqrt{3}}\right)\hat{y} \right] \quad (20)$$

$$\mathbf{g}_2^{tri} \approx \frac{2\pi}{a} \left[ \left(-1 + \epsilon_{xx} - \frac{\epsilon_{xy}}{\sqrt{3}}\right)\hat{x} + \left(\frac{1}{\sqrt{3}} + \epsilon_{xy} - \frac{\epsilon_{yy}}{\sqrt{3}}\right)\hat{y} \right] \quad (21)$$

for the triangular lattice.

#### 2.5. Low-pass filtering

PyAtoms is equipped with a low-pass Gaussian filter option that eliminates short spatial frequencies in an image while preserving long wavelength periodicities. This option is useful in simulating STM images of moiré lattices, where it can be used to remove the atomic lattice, which may not be present in experimental data, either due to the scan size or the particular tunneling conditions. The low-pass filter can

also be used to remove common aliasing effects present in STM data.

For computational efficiency and speed, the low-pass filter in PyAtoms is performed in reciprocal space by taking the product of a Gaussian mask with reciprocal-space width  $\sigma_K$  and the 2D Fourier transform of the atomic image and then inverse Fourier transforming to real-space. The Gaussian mask is given by

$$\Gamma_K = \frac{1}{2\pi\sigma_K} e^{-r^2/2\sigma_K^2}, \quad (22)$$

where the real-space Gaussian width of the filter is given by  $\sigma_R = 1/\sigma_K$ .

### 3. PyAtoms Overview

Figure 3 displays the PyAtoms interface. Below we briefly describe the functionality of each.

**(a,b,c) Lattice 1,2,3:** In the **Lattices** section, users select the properties for each constituent layer. In the **Parameters** tab users select: the lattice symmetry (triangular/hexagonal or square), which sets the primitive lattice vectors; the lattice constant, in nanometers; and twist angle ( $\theta_{12}, \theta_{23}$ ) for two- or three-layer systems. For triangular/hexagonal systems, the **Sublattices** tab allows users to select: the lattice site at the image origin (hollow, A, or B) and the amplitude of each sublattice ( $\alpha_i, \beta_i$ ) (see Fig. 1). In the **Strain** tab, users have the option to apply a 2D strain tensor (Eq. 17), where the  $x$ -axis of strain tensor for  $i$ th layer is along the direction of the  $i$ th layer's first reciprocal lattice vector,  $\mathbf{g}_1^i$  (Eqs. 3, 4).

**(d) Number of lattices:** Here, users select the number of layers/lattices to simulate: single, bi-, or tri-layer lattice as well as the model for approximating the combined system ("Simple" or "Log") and the corresponding parameters ( $\eta, \xi$ ).

**(e) Image parameters:** This section sets the configuration and resolution of the entire image and closely follows typical parameters in STM data collection software. Key image parameters include the number of pixels, the length of the image (in nanometers) and the scan angle,  $\theta$ , which is along the first reciprocal lattice vector of the 1st layer,  $\mathbf{g}_1^1$ , and the image offset,  $(x_0, y_0)$ , where both are real numbers that set the origin of the image. The image parameters tab features a real-time calculation of the resolution in real-space, defined by  $\delta R = L/(N_{pix} - 1)$ , where  $N_{pix}$  is the number of pixels, and the reciprocal space resolution given by  $\delta K = 2\pi/L$ . These values are useful when using PyAtoms for preparing for time-consuming QPI measurements in order to make sure

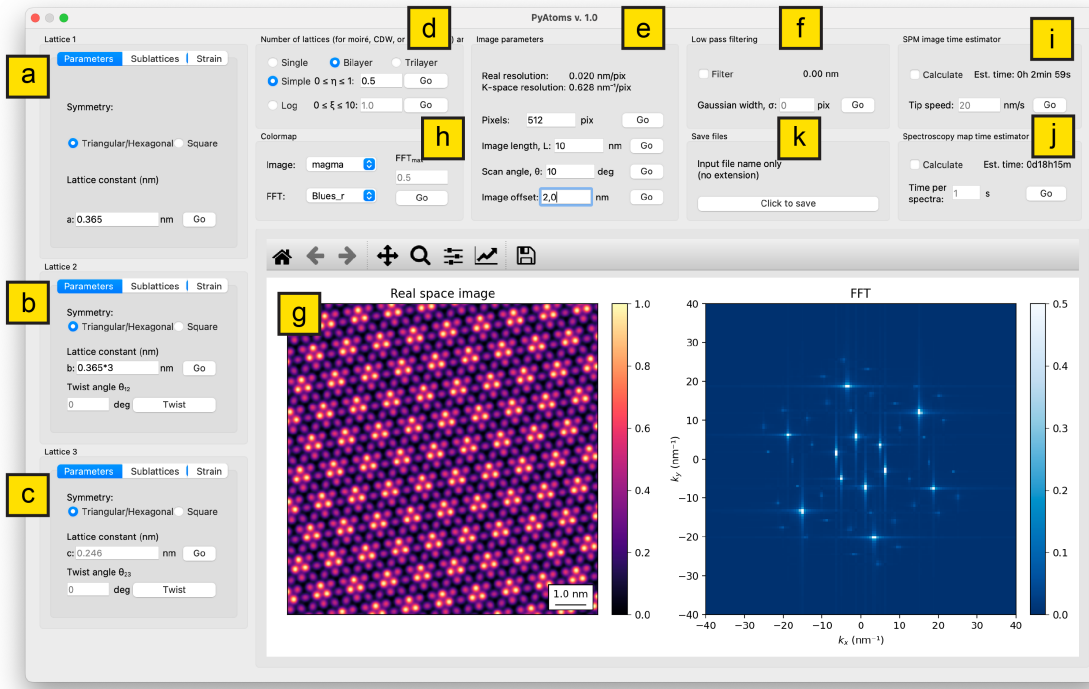


Figure 3. PyAtoms graphical user interface. See text for brief descriptions of each labeled window.

that the pixel sampling rate is above the Nyquist frequency.

**(f) Low pass filtering:** For multilayer simulations, users have the option input a value for `sigma`, the radius of Gaussian mask in real space (pixels) units. The full-width at half-max (FWHM) of the gaussian filter is shown as a white circle in the bottom left corner of the real space image. Likewise, the FWHM of the gaussian filter in reciprocal space is shown as a red circle in the FFT (Fig. 4(d,f)). The radius of the gaussian mask in nanometers is shown in real-time in the text box.

**(g) Imaging window:** This window displays the real-time simulated real-space and reciprocal-space images of the resultant lattice system. The navigation buttons allow the user to zoom, pan, and tune each plot’s image scale. The save button outputs a screenshot of this imaging window, including all axes and text.

**(h) Colormap:** This section enables users to choose the colormap for the real space and FFT images. Additionally, users have the option to set the maximum value of the FFT colormap to enhance less pronounced features.

**(i) SPM image time estimator:** This section estimates the time required to complete scanning of an image, using the values in the `Parameters` tab along

with the scan/tip speed,  $v_t$  (in nanometers/second). This is calculated assuming the SPM tip scans in the left/right fast-scan direction and in a single slow-scan direction (upwards, for example). This time is estimated via

$$T_{im} = 2N_{pix}L/v_t \quad (23)$$

where  $N_{pix}$  is the number of pixels in one line,  $L$  is the length of the image in nanometers,  $v_t$  is the velocity (in nm/s) of the tip in one direction and the factor of 2 takes into account both the left and right fast-scan directions. This section is useful in estimating the time to record a “closed-feedback”  $dI/dV_b$  map where the LDOS( $eV_b$ ) is recorded at a single energy as the tip slowly scans the surface.

**(j) Spectroscopy map time estimator:** This section estimates the time required to complete a pixel-by-pixel square grid spectroscopy map using the values in the `Parameters` tab along with the time (in seconds) that each spectra requires,  $T_{spec}$ . We also assume that spectra are recorded in one direction along both the fast- and slow-scan direction. The time is estimated via

$$T_{map} = N_{pix}^2 T_{spec} + 2N_{pix}L/v_t \quad (24)$$

The user inputs the time per spectra, which is the total time in seconds (including overhead) to record a single spectrum,  $T_{spec}$ , i.e., one  $dI/dV_b$  sweep. This section is useful in estimating the time to record an “open-feedback” LDOS( $eV_b$ ) map where a  $dI/dV_b(V_b)$  spectra



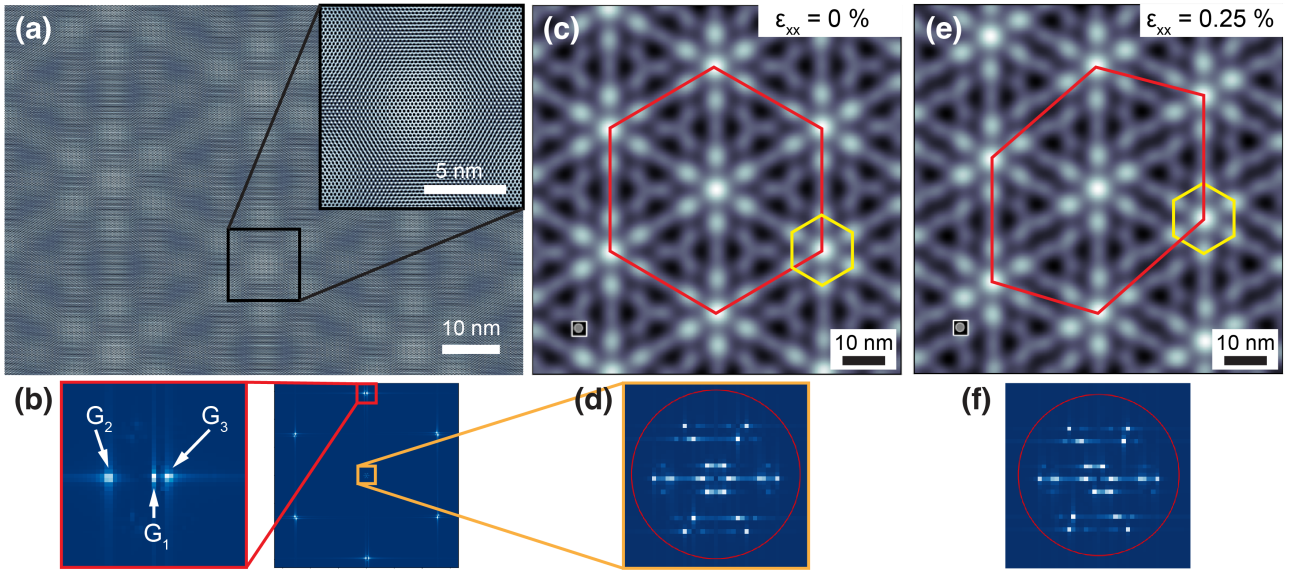


**Figure 4. Twisted trilayer graphene simulation.** (a) Cropped image of a PyAtoms simulation of unstrained twisted trilayer graphene: 2048 pixels,  $a = 2.46 \text{ \AA}$ ,  $L = 90 \text{ nm}$ ,  $\theta_{12} = 1.42^\circ$ ,  $\theta_{23} = -1.88^\circ$ , moiré ‘Simple’ mode. Inset: Atomic-scale zoom on AAA region. (b) (Right) Full-scale FFT of (a) and (Left) detail zoom showing the Bragg peaks for each graphene layer. (c) Low-pass filtered image of (a):  $\sigma_R = 20$  pixels (0.88 nm). The solid lines highlight the nearest-neighbors for the long (red) and short (yellow) moiré wavelength. (d) Zoom FFT of (c) near the origin. The circle displays the filtered region in  $k$ -space. (e) Same as (c) with a small strain on  $G_1$  that warps the moiré pattern. (f) FFT of the strained trilayer graphene.

is recorded at every pixel position. Together with the imaging window (Fig. 3(g)) provided by PyAtoms, this estimator is invaluable in ensuring that time-consuming QPI measurements will have the requisite reciprocal space resolution and spatial extent while avoiding aliasing effects.

**(k) Save Files:** This operation generates a folder named `FileName` containing four files: a PNG file of the real space image, a PNG file of the FFT, a text file containing the key PyAtoms parameters, and a tab-delimited text file containing the real space image in a 2D array that can easily be imported for further analysis.

## 4. Applications

### 4.1. Research

With its simple and real-time GUI interface, PyAtoms is a powerful research tool during STM data collection as well as for data analysis. As shown in Fig. 2, PyAtoms can be used side-by-side during STM measurements in order to rapidly simulate experimental images and determine properties such as the constituent lattice constants and moiré twist angles between layers. Below we describe two examples of PyAtoms research capabilities.

In practice, the strain tuning capabilities of PyAtoms can be used to simulate and determine

the amount of true, physical strain in STM images or the apparent strain due to scan artifacts such as tip drift. Figure 4 demonstrates the dramatic effect that strain can have on the moiré lattice and how PyAtoms’ can be used to determine this strain. Fig. 4(a) is a simulation of twisted trilayer graphene ( $\theta_{12} = 1.42^\circ, \theta_{23} = -1.88^\circ$ ) moiré quasicrystal [43] that features two moiré lattices. The atomic Bragg peaks for each graphene layer can be seen in the Fourier transform (Fig. 4(b)). The complex spatial structure of the moiré -of- moiré pattern (Fig. 4(c)) can be better seen after low-pass filtering to keep only the long wavelength periodicities (Fig. 4(d)). The presence of even minuscule strain in the top-most graphene layer ( $\epsilon_{xx} = 0.25\%$ ) significantly alters the larger moiré pattern in both real (Fig. 4(e)) and reciprocal space (4(f)). For researchers studying moiré multi-layers, PyAtoms can thus be used side-by-side during measurements to quickly determine the local strain in an area so that users can make informed decisions whether to seek other, less-strained areas.

Beyond moiré systems, PyAtoms is especially useful in simulating charge- or bond-density wave systems (CDW/BDW) of various geometries and phases. Figure 5(a,e) displays a simulation of  $2H\text{-NbSe}_2$ , a transition metal dichalcogenide (TMDC) van der Waals crystal that hosts a nearly commensurate CDW [44] with order that is approximately  $(3 \times 3)R0^\circ$  and is shown with a site-centered (left) and bond-

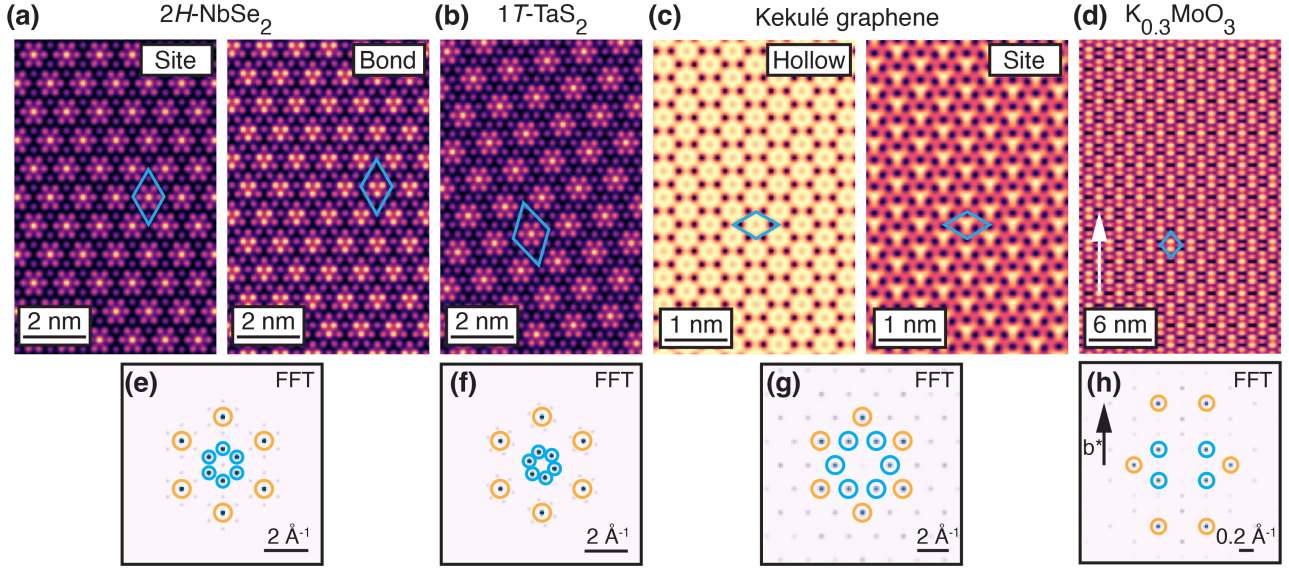


**Figure 5. Site- and bond-centered charge density wave simulations.** (a) Simulation of the approximately  $(3 \times 3)R0^\circ$  CDW in  $2H\text{-NbSe}_2$  ( $a = 3.44 \text{ \AA}$ ) which can be Se site- (left) or bond-centered (right). (b) “Star-of-David”  $(\sqrt{13} \times \sqrt{13})R13.9^\circ$  CDW in  $1T\text{-TaS}_2$  ( $a = 3.36 \text{ \AA}$ ). (c) Kekulé-distorted graphene with  $(\sqrt{3} \times \sqrt{3})R30^\circ$  bond-density wave texture which can be hollow- (left) or C site-centered (right). (d) Incommensurate CDW in quasi-1D  $\text{K}_{0.3}\text{MoO}_3$ , potassium blue bronze. (e)-(h) The respective Fourier transforms. The atomic peaks (yellow) and CDW peaks (blue) are highlighted. (a)-(b) simulated with “Simple” model ( $\eta = 0.3$ ); (c) and (d) simulated with “Log” model using  $\xi = 0$  and  $\xi = 1$ , respectively.

centered (right) CDW phase. Figure 5(b,f) displays the  $(\sqrt{13} \times \sqrt{13})R13.9^\circ$  CDW of TMDC  $1T\text{-TaS}_2$ . Figure 5(c,g) displays simulations of graphene with a  $(\sqrt{3} \times \sqrt{3})R30^\circ$  BDW, termed a Kekulé distortion with a phase centered at a hollow site (“Kekule-O,” left) [45, 46] or carbon site (“Kekulé-Y,” right) [7, 46]. Finally, we show that PyAtoms can also be used to model the CDW in quasi-1D Peierls system  $\text{K}_{0.3}\text{MoO}_3$ , potassium blue bronze [47, 48]. Fig. 5(d) shows the monoclinic atomic lattice projected onto the  $(\bar{2}01)$  surface, which is what is measured by STM [48]. The surface structure is simulated by a strained triangular lattice ( $a_1 = 7.67 \text{ \AA}$ ,  $\epsilon_{yy} = 32\%$ , image scan angle  $\theta = 90^\circ$ ). The nearly commensurate CDW, has a projection along the vertical chain direction (white arrow) ( $|\mathbf{q}_{CDW}^b|/|\mathbf{b}^*| = 0.25$ ) for the  $(\bar{2}01)$  surface [47, 48] and is simulated with a strained square lattice ( $b_1 = 1.39 \text{ nm}$ ,  $\epsilon_{xx} = \epsilon_{xy} = \epsilon_{yy} = 18\%$ ,  $\theta_{12} = 45^\circ$ ). This robust capability to simulate several families of CDW/BDW systems is especially useful when combined with the spectroscopic map time estimators (Fig. 3(i,j)) which allows users to efficiently plan detailed spectroscopic QPI measurements of quantum materials.

#### 4.2. PyAtoms in education

PyAtoms’ speed and user-friendly interface makes it a unique interactive educational tool for teaching fundamental concepts in Fourier analysis and crystal struc-

ture. One of us (C.G.) has used PyAtoms as part of lecture demonstrations in two different undergraduate courses: sophomore-level “Mathematical Methods for Physicists” and senior-level “Introduction to Solid State Physics.” In the maths course, PyAtoms’ real-time imaging of the real- and reciprocal-space structures was used to convey concepts in 2D Fourier analysis, including the real- and reciprocal representation of plane waves and the concept of aliasing. Hiding half of the screen, students would be presented with either a real-space image and asked to determine the Fourier-space structure, or vice versa. In the solid state course, PyAtoms has been used in lecture to reinforce concepts in crystal structure, such as determining the primitive direct and reciprocal lattice vectors. It has also been used to connect students to modern concepts in 2D materials, such as moiré systems.

To illustrate the value of PyAtoms to solid state physics education, consider the problem of determining both the lattice and commensurate superlattice parameters ( $n, \phi$ ) for the system shown in Fig. 6. Here, students are provided the raw text data generated by PyAtoms and are tasked with importing and visualizing the data and calculating the 2D Fourier transform.

*Question:* The data contains both a lattice and a superlattice. What are the primitive lattice vectors for each lattice? What values of  $(n, \phi)$  describe the superlattice?

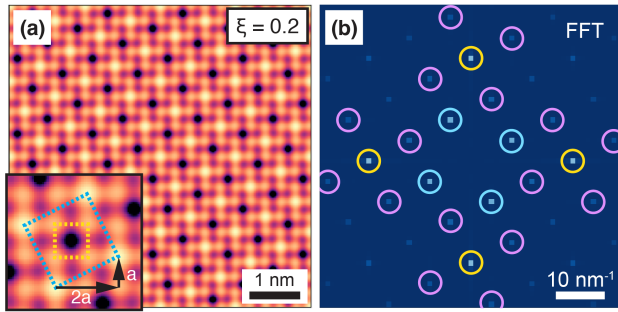


**Figure 6. Square superlattice.** (a) PyAtoms simulation of a square superlattice  $(\sqrt{5} \times \sqrt{5})R26.57^\circ$ . Inset: Zoom view of the smaller square lattice ( $a_1 = 3 \text{ \AA}$ , yellow square) and the  $(\sqrt{5} \times \sqrt{5})R26.57^\circ$  superlattice ( $a_2 = 3 \times \sqrt{5} \approx 6.71 \text{ \AA}$ , blue square). (b) FFT of the image in (a). Yellow circles denote the atomic Bragg peaks; light blue circles denote the 1st order superlattice peaks and light purple the satellite superlattice peaks.

*Solution:* Real and FFT analysis of Fig. 6 shows that the smaller, atomic lattice is a square lattice with primitive lattice vectors given by  $\mathbf{a}_1 = a\hat{x}$  and  $\mathbf{a}_2 = a\hat{y}$ , where  $a = 3 \text{ \AA}$ . By visual inspection of Fig. 6 (inset), one sees that the square superlattice vectors are given by  $\mathbf{b}_1 = 2\mathbf{a}_1 + \mathbf{a}_2$  and  $\mathbf{b}_2 = -\mathbf{a}_1 + 2\mathbf{a}_2$ . The objective is to first determine  $n$ , which is the magnitude of  $\mathbf{b}_1$ :

$$\begin{aligned} \mathbf{b}_1 &= 2a\hat{x} + a\hat{y} \\ \Rightarrow |\mathbf{b}_1| &= \sqrt{2^2 + 1^2}a = \sqrt{5}a. \end{aligned}$$

The orientation of the superlattice with respect to the original,  $\phi$ , is then given by simple geometry:

$$\begin{aligned} \tan \phi &= \frac{b_{1x}}{b_{1y}} = \frac{1}{2} \Rightarrow \phi = \arctan \frac{1}{2} \approx 26.57^\circ \\ \Rightarrow n &= \sqrt{5}, \phi = 26.57^\circ \end{aligned}$$

Problem sets containing this  $(\sqrt{5} \times \sqrt{5})R26.57^\circ$  square system and other superlattices (see Fig. 5) have been assigned in senior-level solid state physics courses at UCLA by C.G. for several years with great success, as determined by post-course evaluations. Here, PyAtoms was used to generate the raw data which students are directed to import, visualize (real and Fourier transformed images) as if it were actual data recorded in an STM laboratory. This example showcases the educational value of PyAtoms, highlighting its practical application in reinforcing theoretical concepts concerning primitive lattice vectors and determining crystal structure as well as inspiring students to develop key programming and data analysis skills. The ease with which complex systems can be simulated, such as multi-layer moiré systems (Fig. 4), offers educators the opportunity to connect their students to concepts in current condensed matter physics research.

## 5. Outlook

We have presented PyAtoms, an interactive open-source Python-based software for the real-time simulation of STM images of 2D materials. With its quick, intuitive, and robust simulation capabilities, we envision PyAtoms as valuable companion during both STM measurements and STM data analysis. PyAtoms can also be used as an educational tool to train new STM researchers as well as in the classroom when covering concepts in Fourier analysis and solid state physics.

Possible future developments include offering other methods for approximating images of multilayer systems and allowing generic 2D lattices to be generated beyond square and triangular. Similarly, for the CDW/BDW simulations, control of the phase in real space would allow easier comparisons to real STM data [6, 31, 32]. A current weakness in PyAtoms, is that comparison to experiment is largely qualitative. However, apart from its GUI, the open-source code that underlies PyAtoms can be called separately (through a Python terminal, for instance) and can be used, for example, to simulate moiré and superlattice systems beyond three layers. In principle, this ability to call on PyAtoms' base functions offers the intriguing possibility to determine the simulation parameters (lattice constant, A- and B-sublattice amplitude, strain) through a least squares fitting to experimental STM data. This latter capability would elevate PyAtoms to a useful quantitative tool in the study of 2D materials.

## Acknowledgments

The authors thank M. Mandigo-Stoba, K.-Y. Wey, and S. Nekarae for providing STM images, F. Joucken for carefully explaining the “Log” method of STM simulation in reference [38], and J. Berger, C. Irving for technical assistance with STM assembly. A.G.P acknowledges financial support from the National Science Foundation (NSF), the UCLA office of the Dean of Physical Sciences through the UCLA Physics Bridge Program and the UCLA Graduate Division through a Eugene Cota-Robles Fellowship. C.G. acknowledges teaching relief support from the UCLA offices of the Executive Vice Chancellor and Provost, Vice Chancellor for Research and Creative Activities, and the Vice Chancellor for Academic Personnel and partial support from the UCLA Hellman Society of Fellows.

## Author contributions

C.G. created the original PyAtoms base codes (`hexatoms`, `squareatoms`, `moirelattice`) in Matlab. A.G.P. translated the base codes from Matlab to



Python and created the GUI interface with input from C.G. Both A.G.P. and C.G. contributed to PyAtoms' later updates. C.G. wrote the manuscript and created the figures with input from A.G.P.

## References

- [1] Gerd Binnig and Heinrich Rohrer. Scanning tunneling microscopy—from birth to adolescence. *Reviews of Modern Physics*, 59(3):615–625, July 1987. Publisher: American Physical Society.
- [2] Kathryn Ann Moler. Imaging quantum materials. *Nature Materials*, 16(11):1049–1052, November 2017. Publisher: Nature Publishing Group.
- [3] Øystein Fischer, Martin Kugler, Ivan Maggio-Aprile, Christophe Berthod, and Christoph Renner. Scanning tunneling spectroscopy of high-temperature superconductors. *Rev. Mod. Phys.*, 79:353–419, Mar 2007.
- [4] J. E. Hoffman, K. McElroy, D.-H. Lee, K. M Lang, H. Eisaki, S. Uchida, and J. C. Davis. Imaging Quasiparticle Interference in  $\text{Bi2Sr2CaCu2O8}+\delta$ . *Science*, 297(5584):1148–1151, August 2002. Publisher: American Association for the Advancement of Science.
- [5] William Sacks, Dmitri Roditchev, and Jean Klein. Voltage-dependent stm image of a charge density wave. *Phys. Rev. B*, 57:13118–13131, May 1998.
- [6] C. J. Arguello, S. P. Chockalingam, E. P. Rosenthal, L. Zhao, C. Gutiérrez, J. H. Kang, W. C. Chung, R. M. Fernandes, S. Jia, A. J. Millis, R. J. Cava, and A. N. Pasupathy. Visualizing the charge density wave transition in  $2\text{H} - \text{NbSe}_2$  in real space. *Physical Review B*, 89(23):235115, June 2014.
- [7] Christopher Gutiérrez, Cheol-Joo Kim, Lola Brown, Theanne Schiros, Dennis Nordlund, Edward B. Lochocki, Kyle M. Shen, Jiwoong Park, and Abhay N. Pasupathy. Imaging chiral symmetry breaking from Kekulé bond order in graphene (S.I.). *Nature Physics*, 12(10):950–958, October 2016.
- [8] Gregory M Rutter, JN Crain, NP Guisinger, T Li, PN First, and JA Stroscio. Scattering and interference in epitaxial graphene. *Science*, 317(5835):219–222, 2007.
- [9] Jiamin Xue, Javier Sanchez-Yamagishi, Danny Bulmash, Philippe Jacquod, Aparna Deshpande, K Watanabe, T Taniguchi, Pablo Jarillo-Herrero, and Brian J LeRoy. Scanning tunnelling microscopy and spectroscopy of ultra-flat graphene on hexagonal boron nitride. *Nature materials*, 10(4):282–285, 2011.
- [10] Régis Decker, Yang Wang, Victor W. Brar, William Regan, Hsin-Zon Tsai, Qiong Wu, William Gannett, Alex Zettl, and Michael F. Crommie. Local Electronic Properties of Graphene on a BN Substrate via Scanning Tunneling Microscopy. *Nano Letters*, 11(6):2291–2295, June 2011. Publisher: American Chemical Society.
- [11] Chendong Zhang, Chih-Piao Chuu, Xibiao Ren, Ming-Yang Li, Lain-Jong Li, Chuanhong Jin, Mei-Yin Chou, and Chih-Kang Shih. Interlayer couplings, Moiré patterns, and 2D electronic superlattices in  $\text{MoS}_2/\text{WSe}_2$  heterobilayers. *Science Advances*, 3(1):e1601459, January 2017. Publisher: American Association for the Advancement of Science.
- [12] Alexander Kerelsky, Leo J. McGilly, Dante M. Kennes, Lede Xian, Matthew Yankowitz, Shaowen Chen, K. Watanabe, T. Taniguchi, James Hone, Cory Dean, Angel Rubio, and Abhay N. Pasupathy. Maximized electron interactions at the magic angle in twisted bilayer graphene. *Nature*, 572(7767):95–100, August 2019.
- [13] Yuhang Jiang, Xinyuan Lai, Kenji Watanabe, Takashi Taniguchi, Kristjan Haule, Jinhai Mao, and Eva Y. Andrei. Charge order and broken rotational symmetry in magic-angle twisted bilayer graphene. *Nature*, 573(7772):91–95, September 2019. Number: 7772 Publisher: Nature Publishing Group.
- [14] Yonglong Xie, Biao Lian, Berthold Jäck, Xiaomeng Liu, Cheng-Li Chiu, Kenji Watanabe, Takashi Taniguchi, B. Andrei Bernevig, and Ali Yazdani. Spectroscopic signatures of many-body correlations in magic-angle twisted bilayer graphene. *Nature*, 572(7767):101–105, August 2019.
- [15] Hongyuan Li, Shaowei Li, Mit H. Naik, Jingxu Xie, Xinyu Li, Jiayin Wang, Emma Regan, Danqing Wang, Wenyu Zhao, Sihan Zhao, Salman Kahn, Kentaro Yumigeta, Mark Blei, Takashi Taniguchi, Kenji Watanabe, Sefaattin Tongay, Alex Zettl, Steven G. Louie, Feng Wang, and Michael F. Crommie. Imaging moiré flat bands in three-dimensional reconstructed  $\text{WSe}_2/\text{WS}_2$  superlattices. *Nature Materials*, 20(7):945–950, July 2021. Bandiera.abtest: a Cg.type: Nature Research Journals Number: 7 Primary\_atype: Research Publisher: Nature Publishing Group Subject\_term: Electronic properties and materials;Imaging techniques;Structure of solids and liquids;Two-dimensional materials Subject\_term.id: electronic-properties-and-materials;imaging-techniques;structure-of-solids-and-liquids;two-dimensional-materials.
- [16] Hyunjin Kim, Youngjoon Choi, Étienne Lantagne-Hurtubise, Cyprian Lewandowski, Alex Thomson, Lingyuan Kong, Haoxin Zhou, Eli Baum, Yiran Zhang, Ludwig Holleis, Kenji Watanabe, Takashi Taniguchi, Andrea F. Young, Jason Alicea, and Stevan Nadj-Perge. Imaging inter-valley coherent order in magic-angle twisted trilayer graphene. *Nature*, 623(7989):942–948, November 2023. Publisher: Nature Publishing Group.
- [17] MR Slot, Yulia Maximenko, Paul M Haney, Sungmin Kim, DT Walkup, Evgheni Strelcov, Son T Le, EM Shih, D Yildiz, SR Blankenship, et al. A quantum ruler for orbital magnetism in moiré quantum matter. *Science*, 382(6666):81–87, 2023.
- [18] Somesh Chandra Ganguli, Markus Aapro, Shawulienu Kezilebieke, Mohammad Amini, Jose L Lado, and Peter Liljeroth. Visualization of moiré magnons in monolayer ferromagnet. *Nano Letters*, 23(8):3412–3417, 2023.
- [19] Nurit Avraham, Jonathan Reiner, Abhay Kumar-Nayak, Noam Morali, Rajib Batabyal, Binghai Yan, and Haim Beidenkopf. Quasiparticle Interference Studies of Quantum Materials. *Advanced Materials*, 30(41):1707628, 2018.
- [20] David Nečas and Petr Klapetek. Gwyddion: an open-source software for SPM data analysis. *Central European Journal of Physics*, 10:181–188, 2012.
- [21] Tara Stephens and Shawna M. Hollen. Moiré pattern simulator.
- [22] Tobias A. de Jong. Moiré lattice generator.
- [23] Kamal Choudhary, Kevin F. Garrity, Charles Camp, Sergei V. Kalinin, Rama Vasudevan, Maxim Ziatdinov, and Francesca Tavazza. Computational scanning tunneling microscope image database. *Scientific Data*, 8(1):57, February 2021. Number: 1 Publisher: Nature Publishing Group.
- [24] Charles R. Harris, K. Jarrod Millman, Stéfan J. van der Walt, Ralf Gommers, Pauli Virtanen, David Cournapeau, Eric Wieser, Julian Taylor, Sebastian Berg, Nathaniel J. Smith, Robert Kern, Matti Picus, Stephan Hoyer, Marten H. van Kerkwijk, Matthew Brett, Allan Haldane, Jaime Fernández del Río, Mark Wiebe, Pearu Peterson, Pierre Gérard-Marchant, Kevin Sheppard, Tyler Reddy, Warren Weckesser, Hameer Abbasi, Christoph Gohlke, and Travis E. Oliphant. Array pro-

- gramming with NumPy. *Nature*, 585(7825):357–362, September 2020. Number: 7825 Publisher: Nature Publishing Group.
- [25] Pauli Virtanen, Ralf Gommers, Travis E. Oliphant, Matt Haberland, Tyler Reddy, David Cournapeau, Evgeni Burovski, Pearu Peterson, Warren Weckesser, Jonathan Bright, Stéfan J. van der Walt, Matthew Brett, Joshua Wilson, K. Jarrod Millman, Nikolay Mayorov, Andrew R. J. Nelson, Eric Jones, Robert Kern, Eric Larson, C. J. Carey, Ílhan at, Yu Feng, Eric W. Moore, Jake VanderPlas, Denis Laxalde, Josef Perktold, Robert Cimrman, Ian Henriksen, E. A. Quintero, Charles R. Harris, Anne M. Archibald, Antônio H. Ribeiro, Fabian Pedregosa, and Paul van Mulbregt. SciPy 1.0: fundamental algorithms for scientific computing in python. 17(3):261–272. Number: 3 Publisher: Nature Publishing Group.
- [26] John D. Hunter. Matplotlib: A 2D Graphics Environment. *Computing in Science & Engineering*, 9(03):90–95, May 2007. Publisher: IEEE Computer Society.
- [27] M. J. Hÿtch, E. Snoeck, and R. Kilaas. Quantitative measurement of displacement and strain fields from HREM micrographs. *Ultramicroscopy*, 74(3):131–146, August 1998.
- [28] M. H. Hamidian, S. D. Edkins, Sang Hyun Joo, A. Kostin, H. Eisaki, S. Uchida, M. J. Lawler, E.-A. Kim, A. P. Mackenzie, K. Fujita, Jinho Lee, and J. C. Séamus Davis. Detection of a Cooper-pair density wave in  $\text{Bi}_2\text{Sr}_2\text{CaCu}_2\text{O}_{8+x}$ . *Nature*, 532(7599):343–347, April 2016. Number: 7599 Publisher: Nature Publishing Group.
- [29] Stefan Hembacher, Franz J Giessibl, Jochen Mannhart, and Calvin F Quate. Revealing the hidden atom in graphite by low-temperature atomic force microscopy. *Proceedings of the National Academy of Sciences*, 100(22):12539–12542, 2003.
- [30] Joseph M. Carpinelli, Hanno H. Weitering, E. Ward Plummer, and Roland Stumpf. Direct observation of a surface charge density wave. *Nature*, 381(6581):398–400, May 1996.
- [31] Árpád Pásztor, Alessandro Scarfato, Marcello Spera, Céline Barreateau, Enrico Giannini, and Christoph Renner. Holographic imaging of the complex charge density wave order parameter (SI). 1(3):033114.
- [32] Shunsuke Yoshizawa, Keisuke Sagisaka, and Hideaki Sakata. Visualization of alternating triangular domains of charge density waves in  $2h\text{-NbSe}_2$  by scanning tunneling microscopy. *Phys. Rev. Lett.*, 132:056401, Jan 2024.
- [33] Yuan Cao, Valla Fatemi, Ahmet Demir, Shiang Fang, Spencer L. Tomarken, Jason Y. Luo, Javier D. Sanchez-Yamagishi, Kenji Watanabe, Takashi Taniguchi, Efthimios Kaxiras, Ray C. Ashoori, and Pablo Jarillo-Herrero. Correlated insulator behaviour at half-filling in magic-angle graphene superlattices. *Nature*, 556(7699):80–84, April 2018.
- [34] Yuan Cao, Valla Fatemi, Shiang Fang, Kenji Watanabe, Takashi Taniguchi, Efthimios Kaxiras, and Pablo Jarillo-Herrero. Unconventional superconductivity in magic-angle graphene superlattices. *Nature*, 556(7699):43–50, April 2018.
- [35] Aaron L. Sharpe, Eli J. Fox, Arthur W. Barnard, Joe Finney, Kenji Watanabe, Takashi Taniguchi, M. A. Kastner, and David Goldhaber-Gordon. Emergent ferromagnetism near three-quarters filling in twisted bilayer graphene. *Science*, 365(6453):605–608, August 2019. Publisher: American Association for the Advancement of Science Section: Report.
- [36] Leon Balents, Cory R Dean, Dmitri K Efetov, and Andrea F Young. Superconductivity and strong correlations in moiré flat bands. *Nature Physics*, 16(7):725–733, 2020.
- [37] Kin Fai Mak and Jie Shan. Semiconductor moiré materials. *Nature Nanotechnology*, 17(7):686–695, 2022.
- [38] Frédéric Joucken, Fernande Frising, and Robert Sporken. Fourier transform analysis of STM images of multilayer graphene moiré patterns. *Carbon*, 83:48–52, March 2015.
- [39] C. R. Woods, L. Britnell, A. Eckmann, R. S. Ma, J. C. Lu, H. M. Guo, X. Lin, G. L. Yu, Y. Cao, R. V. Gorbachev, A. V. Kretinin, J. Park, L. A. Ponomarenko, M. I. Katsnelson, Yu N. Gornostyrev, K. Watanabe, T. Taniguchi, C. Casiraghi, H.-J. Gao, A. K. Geim, and K. S. Novoselov. Commensurate-incommensurate transition in graphene on hexagonal boron nitride. *Nature Physics*, 10(6):451–456, June 2014. Publisher: Nature Publishing Group.
- [40] Guohong Li, Adina Luican, and Eva Y. Andrei. Scanning Tunneling Spectroscopy of Graphene on Graphite. *Physical Review Letters*, 102(17):176804, April 2009. Publisher: American Physical Society.
- [41] Guohong Li, A. Luican, J. M. B. Lopes dos Santos, A. H. Castro Neto, A. Reina, J. Kong, and E. Y. Andrei. Observation of Van Hove singularities in twisted graphene layers. *Nature Physics*, 6(2):109–113, February 2010. Publisher: Nature Publishing Group.
- [42] Vitor M. Pereira, A. H. Castro Neto, and N. M. R. Peres. Tight-binding approach to uniaxial strain in graphene. *Physical Review B*, 80(4):045401, July 2009. Publisher: American Physical Society.
- [43] Aviram Uri, Sergio C. de la Barrera, Mallika T. Randeria, Daniel Rodan-Legrain, Trithep Devakul, Philip J. D. Crowley, Nisarga Paul, Kenji Watanabe, Takashi Taniguchi, Ron Lifshitz, Liang Fu, Raymond C. Ashoori, and Pablo Jarillo-Herrero. Superconductivity and strong interactions in a tunable moiré quasicrystal. *Nature*, 620(7975):762–767, August 2023. Publisher: Nature Publishing Group.
- [44] D. E. Moncton, J. D. Axe, and F. J. DiSalvo. Neutron scattering study of the charge-density wave transitions in  $2\text{H-TaSe}_2$  and  $2\text{H-NbSe}_2$ . *Physical Review B*, 16(2):801–819, July 1977. Publisher: American Physical Society.
- [45] Si-Yu Li, Yu Zhang, Long-Jing Yin, and Lin He. Scanning tunneling microscope study of quantum Hall isospin ferromagnetic states in the zero Landau level in a graphene monolayer. *Physical Review B*, 100(8):085437, August 2019. Publisher: American Physical Society.
- [46] Kevin P. Nuckolls, Ryan L. Lee, Myungchul Oh, Dillon Wong, Tomohiro Soejima, Jung Pyo Hong, Dumitru Călugăru, Jonah Herzog-Arbeitman, B. Andrei Bernevig, Kenji Watanabe, Takashi Taniguchi, Nicolas Regnault, Michael P. Zaletel, and Ali Yazdani. Quantum textures of the many-body wavefunctions in magic-angle graphene. *Nature*, 620(7974):525–532, August 2023.
- [47] G. Travaglini, P. Wachter, J. Marcus, and C. Schlenker. The blue bronze  $\text{K}_0.3\text{MoO}_3$ : A new one-dimensional conductor. *Solid State Communications*, 37(7):599–603, February 1981.
- [48] C. Brun, J. C. Girard, Z. Z. Wang, J. Marcus, J. Dumas, and C. Schlenker. Charge-density waves in rubidium blue bronze  $\text{Rb}_{0.3}\text{MoO}_3$  observed by scanning tunneling microscopy. *Physical Review B*, 72(23):235119, December 2005. Publisher: American Physical Society.